Raman scattering study of NaFe$_{0.53}$Cu$_{0.47}$As

W.-L. Zhang,[1,*] Y. Song,[2] W.-Y. Wang,[2] C.-D. Cao,[2,†] P.-C. Dai,[2] C.-Q. Jin,[3,4] and G. Blumberg[1,5,‡]

[1]*Department of Physics & Astronomy, Rutgers University, Piscataway, New Jersey 08854, USA*
[2]*Department of Physics and Astronomy and Rice Center for Quantum Materials, Rice University, Houston, Texas 77005, USA*
[3]*Beijing National Laboratory for Condensed Matter Physics and Institute of Physics, Chinese Academy of Sciences, Beijing 100190, China*
[4]*Collaborative Innovation Center of Quantum Matter, Beijing, China*
[5]*National Institute of Chemical Physics and Biophysics, Akadeemia tee 23, 12618 Tallinn, Estonia*

We use polarization-resolved Raman scattering to study lattice dynamics in NaFe$_{0.53}$Cu$_{0.47}$As single crystals. We identify four A_{1g} phonon modes, at 126, 172, 183, and 197 cm^{-1}, and four B_{3g} phonon modes at 101, 139, 173, and 226 cm^{-1} (D_{4h} point group). The phonon spectra are consistent with the *Ibam* space group, which confirms that the Cu and Fe atoms form a stripe order. The temperature dependence of the phonon spectra suggests weak electron-phonon and magnetoelastic interactions.

I. INTRODUCTION

The parent compound of the iron-pnictide superconductor, NaFeAs, is a "bad metal." It exhibits a tetragonal-to-orthorhombic transition at 52 K, a paramagnetic–to–spin-density-wave transition at 41 K, and a superconducting transition at 23 K [1]. Doping copper into NaFeAs suppresses both the orthorhombic and the paramagnetic–to–spin-density-wave orders and enhances the superconductivity [2–4]. Recently, it was shown that heavy Cu substitution at the Fe site induces Mott-insulator-like behavior [5,6]. The electronic properties of the heavily doped NaFe$_{1-x}$Cu$_x$As are similar to those of lightly doped cuprates [5,7,8].

For Cu substitution concentration $x > 0.44$ a long-range collinear antiferromagnetic order with magnetic moments residing only at the Fe sites develops below 200 K. The moment increases with Cu concentration substitution x [6]. At the solubility limit near $x = 0.5$, new superlattice peaks appear in the TEM diffraction pattern, which are interpreted as the signature of Cu and Fe stripe-order formation [6], as depicted in the inset in Fig. 1. Compared to the parent NaFeAs compound in the tetragonal phase, the stripe-ordering of Cu and Fe in heavily doped NaFe$_{1-x}$Cu$_x$As removes the lattice fourfold rotational symmetry and reduces the crystallographic space group from *Fmmm* (point group D_{4h}) to *Ibam* (point group D_{2h}), making a structural analog of the magnetic order in parent NaFeAs crystals.

Here we present a polarization-resolved Raman scattering study of the lattice dynamics for NaFe$_{0.53}$Cu$_{0.47}$As single crystals. Four A_g phonon modes, at 126, 172, 183, and 197 cm^{-1}, and four B_{3g} phonon modes at 101, 139, 173, and 226 cm^{-1}, are identified. The phonon spectra are consistent with the Fe/Cu stripe-ordered structure. All the observed phonons exhibit a symmetric line shape. Across the antiferromagnetic phase transition, no phonon anomaly is observed. The data suggest weak electron-phonon and magnetoelastic interaction.

II. EXPERIMENTAL

NaFe$_{1-x}$Cu$_x$As single crystals were grown by the self-flux method [6,9]. The nominal Cu concentration was $x = 0.85$, which resulted in an actual concentration $x = 0.47$ [6]. The
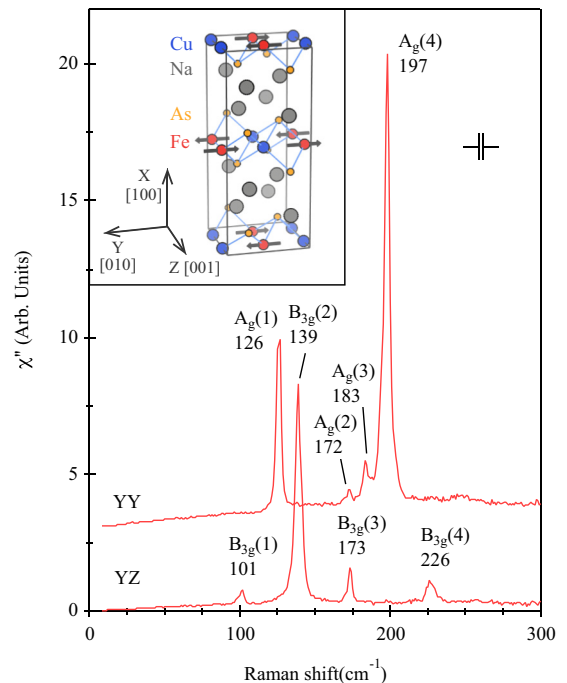

FIG. 1. Raman scattering spectra from NaFe$_{0.53}$Cu$_{0.47}$As crystal for YY + ZZ and YZ + ZY scattering geometries at 250 K measured with 1.9 eV excitation. The spectral resolution is 2.5 cm^{-1}. Inset: NaFe$_{0.5}$Cu$_{0.5}$As unit cell with Cu and Fe collinear stripe order. Arrows at the Fe sites mark magnetic moments.

*wz131@physics.rutgers.edu
†Present address: Department of Applied Physics, Northwestern Polytechnical University, Xian 710072, China.
‡girsh@physics.rutgers.edu

TABLE I. Phonon mode decomposition at the Γ point and selection rules for Raman-active modes in the *Ibam* space group.

		Irreducible representation
Acoustic		$B_{1u} + B_{2u} + B_{3u}$
IR		$3B_{1u} + 5B_{2u} + 5B_{3u}$
Raman		$4A_g + 6B_{1g} + 4B_{2g} + 4B_{3g}$
Silent		$2A_u$
Atom	Wyckoff position	Raman-active mode
Na	$8j$	$2A_g + 2B_{1g} + B_{2g} + B_{3g}$
Fe	$4b$	$B_{1g} + B_{2g} + B_{3g}$
Cu	$4a$	$B_{1g} + B_{2g} + B_{3g}$
As	$8j$	$2A_g + 2B_{1g} + B_{2g} + B_{3g}$

preparation of the reference LiFeAs single crystal is described in [10].

The NaFe$_{1-x}$Cu$_x$As crystal belongs to the *Ibam* space group at room temperature, as shown in the inset in Fig. 1. The crystallographic principal axis [001] of the *Ibam* group is along the Fe(Cu) stripe direction. We define the X, Y, and Z axes along crystallographic [100], [010], and [001] axes and Y′/Z′ along the [011]/[0$\bar{1}$1] direction [inset Fig. 2(a)].

There are 12 atoms in the primitive unit cell. Group theoretical analysis infers $4A_g + 6B_{1g} + 4B_{2g} + 4B_{3g} + 2A_u + 4B_{1u} + 6B_{2u} + 6B_{3u}$ [11] symmetry decomposition of the 36 phonon modes at the Brillouin zone center Γ point. All the even g modes are Raman active. The irreducible representations and decomposition of the Raman active modes by symmetry are summarized in Table I.

Polarization-resolved low-temperature Raman scattering measurements were performed in a quasibackscattering setup from a natural cleaved (100) surface [12]. Polarizers with an extinction ratio better than 1:500 were employed [13]. Samples were cleaved in a nitrogen-filled glove bag and immediately transferred to an optical cryostat with continuous helium gas flow. We used 1.9 and 2.6 eV excitations from a Kr$^+$ laser, where the laser was focused on a 50×50-μm^2 spot on the sample. The power was kept below 10 mW to minimize the laser heating. The local laser heating was estimated [14,15] and kept at less than 5 K. All referred temperatures are corrected for the laser heating.

The Raman scattering signal was analyzed with a triple-stage spectrometer with the spectral resolution setting at about 2 cm^{-1}. We used scattering geometries $\mu\nu$ with $\mu/\nu =$ Y, Z, Y′, and Z′, where $\mu\nu$ is short for $\bar{X}(\mu\nu)$X in Porto's notation. All spectra were corrected for the spectral response to obtain the Raman scattering intensity $I_{\mu\nu}(\omega, T)$. The Raman susceptibility $\chi''_{\mu\nu}(\omega, T)$ was related to $I_{\mu\nu}(\omega, T)$ by $I_{\mu\nu}(\omega, T) = \chi''_{\mu\nu}(\omega, T)[1 + n(\omega, T)]$, where $n(\omega, T)$ is the Bose factor.

In Table II we list the Raman tensor for the D_{2h} group and the selection rule for experimentally accessible polarizations [16]. Due to the twin structure [6], the collected signal from the (100) surface is a superposition of Raman scattering intensities from two types of orthogonal domains. For example, the signal for parallel polarized scattering geometry along the crystallographic axes contains the intensity from YY geometry for one type of domain and ZZ geometry for the other type of domain. We denote this scattering geometry YY + ZZ. Similarly, cross-polarized signal along the crystallographic
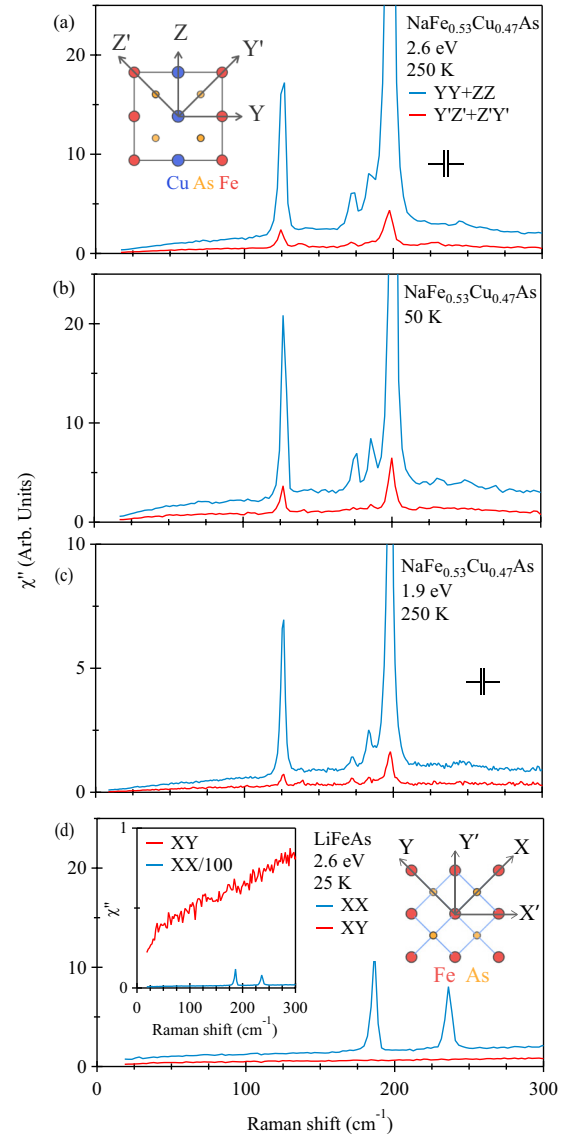

FIG. 2. (a, b) A_g-symmetry Raman active phonon modes measured for NaFe$_{0.53}$Cu$_{0.47}$As crystal at (a) 250 K and (b) 50 K in YY + ZZ (blue line) and Y′Z′ + Z′Y′ (red line) scattering geometries with 2.6 eV laser excitation and spectral resolution 3.5 cm^{-1}. Inset in (a): Top view of the Fe-Cu-As layer for the NaFe$_{0.53}$Cu$_{0.47}$As structure and the YZ-Y′Z′ coordinates. (c) The same A_g phonon modes measured at 250 K with 1.9-eV excitation. (d) Raman spectra from tetragonal LiFeAs crystal at 25 K measured in X′X′ (blue line) and XY (red line) scattering geometries with 2.6 eV laser excitation. Inset in (d). Left: Zoom-in of the data where the signal for X′X′ polarization is divided by 100 to demonstrate the lack of detectable leakage into cross polarization. Right: Top view of the Fe-As layer for the LiFeAs crystal structure and the XY-X′Y′ coordinates.

axes contains contributions from YZ and ZY geometries and is denoted YZ + ZY, and cross-polarized signal along the diagonal directions contains contributions from Y′Z′ and Z′Y′ scattering geometries and is denoted Y′Z′ + Z′Y′.

Following the notation in Table II, we assign all phonons that appear in the YY + ZZ geometry to the A_g symmetry modes, and those appear in the YZ + ZY geometry to the B_{3g} modes.

TABLE II. Raman tensor and selection rules for Raman-active modes in the D_{2h} point group.

$$R_{A_g} = \begin{bmatrix} a & 0 & 0 \\ 0 & b & 0 \\ 0 & 0 & c \end{bmatrix} \qquad R_{B_{1g}} = \begin{bmatrix} 0 & d & 0 \\ e & 0 & 0 \\ 0 & 0 & 0 \end{bmatrix}$$

$$R_{B_{2g}} = \begin{bmatrix} 0 & 0 & f \\ 0 & 0 & 0 \\ g & 0 & 0 \end{bmatrix} \qquad R_{B_{3g}} = \begin{bmatrix} 0 & 0 & 0 \\ 0 & 0 & h \\ 0 & i & 0 \end{bmatrix}$$

(001) surface	XX	YY	XY/YX	
A_g	a^2	b^2	0	
B_{1g}	0	0	d^2/e^2	
(010) surface	XX	ZZ	XZ/ZX	
A_g	a^2	c^2	0	
B_{2g}	0	0	f^2/g^2	
(100) surface	YY/ZZ	YZ/ZY	Y'Y'/Z'Z'	Y'Z'/Z'Y'
A_g	b^2/c^2	0	$(b+c)^2/4$	$(b-c)^2/4$
B_{3g}	0	h^2/i^2	$(h+i)^2/4$	$(h-i)^2/4$

III. RESULTS AND DISCUSSIONS

In Fig. 1 we show the Raman response for NaFe$_{0.53}$Cu$_{0.47}$As crystals at 250 K for YY + ZZ and YZ + ZY scattering geometries. We identify all the A_g and B_{3g} phonon modes predicted by group theory: four A_g symmetry modes, at 126, 172, 183, and 197 cm^{-1}, and four B_{3g} symmetry modes, at 101, 139, 173, and 226 cm^{-1}. All modes show a symmetric line shape.

We note that at the same frequency as the A_g phonon modes, some modes with a weaker intensity are also observed for the Y'Z' + Z'Y' geometry for both 2.6 and 1.9 eV laser excitations [Figs. 2(a)–2(c)]. The intensity of the leaking modes is about 10% of the A_g phonon intensity in the YY + ZZ geometry, which is much higher than the experimental polarization extinction ratio. In Fig. 2(d) we show data for the LiFeAs tetragonal structure [17] measured employing the same setup. If the substituted Cu ions at Fe sites were randomly disordered, the NaFe$_{1-x}$Cu$_x$As structure would have the same point-group symmetry as the LiFeAs structure. By symmetry, no Raman-active phonons are allowed in the XY scattering geometry for the LiFeAs structure. As we demonstrate in the inset in Fig. 2(d), the leakage intensity for the tetragonal LiFeAs structure is less than a percent.

Based on the Raman scattering selection rules, we can deduce that the leakage intensity is proportional to $(b-c)^2/4$ (Table I), which is a measure of the anisotropic electronic properties between the Y and the Z directions [15]. The observation of leakage is consistent with the suggested formation of a long-range stripe order which breaks the crystallographic fourfold symmetry [6]. The count of observed Raman-active phonons for the NaFe$_{1-x}$Cu$_x$As structure also suggests that the size of its primitive cell is four times larger than that for the NaFeAs structure (Table I), therefore, the only possible consistent structure is the Fe-Cu stripe-order phase, as shown in the inset in Fig. 1.

In Figs. 3(a) and 3(b) we show the intensity plot of the Raman response $\chi''(\omega, T)$ for A_g (YY + ZZ) and B_{3g} (YZ + ZY) symmetry channels between 250 and 60 K. All phonons show a symmetric line shape. The number of phonon modes
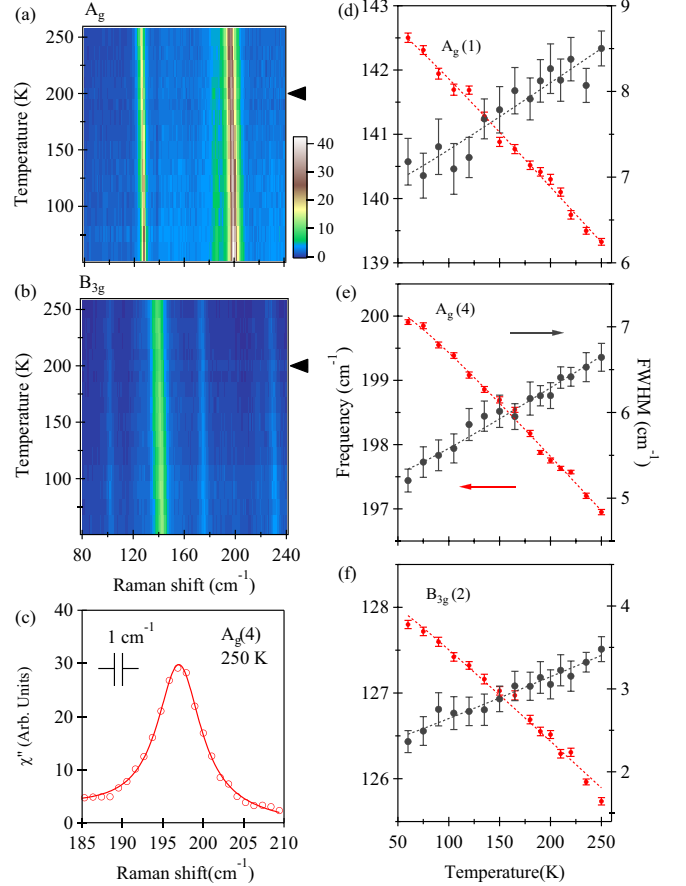

FIG. 3. For NaFe$_{0.53}$Cu$_{0.47}$As crystals, temperature dependence of the Raman response in (a) A_g and (b) B_{3g} symmetry channels measured with 1.9 eV laser excitation. The spectral resolution is 1 cm^{-1}. Black arrows indicate the magnetic phase transition at 200 K. (c) Lorentz fit to the $A_g(4)$ phonon at 250 K. Inset: Spectral resolution. (d–f) Temperature dependence of the phonon peak frequency for the $A_g(1)$, $A_g(4)$, and $B_{3g}(2)$ modes. Vertical error bars are one standard deviation error of the Lorentzian fit. Dashed lines show fits of the phonon frequency and line width to Eqs. (1) and (2).

and their line shapes do not change across the antiferromagnetic phase transition at 200 K, suggesting weak magnetoelastic interaction.

We analyze $A_g(1)$, $A_g(4)$, and $B_{3g}(2)$ phonons by fitting to Lorentzian function. As an example, Fig. 3(c) shows the $A_g(4)$ mode at 250 K and its Lorentzian fit. The fitting results are summarized in Figs. 3(d) and 3(e). Since the magnetoelastic interaction appears to be undetectable within the experimental resolution, we fit the mode's temperature dependence by the anharmonic decay model for the entire temperature range (250 to 60 K) [18]:

$$\omega(T) = \omega_0 - \omega_1 \left[1 + \frac{2}{e^{\hbar\omega_0/2k_B T} - 1} \right] \qquad (1)$$

$$\Gamma(T) = \Gamma_0 + \Gamma_1 \left[1 + \frac{2}{e^{\hbar\omega_0/2k_B T} - 1} \right] \qquad (2)$$

The fitting results are summarized in Table III.

TABLE III. Fitting parameters for the frequency and line width of the $A_g(1)$, $A_g(4)$, and $B_{3g}(2)$ modes. Units are cm^{-1}.

Mode	ω_0	ω_1	$2\Gamma_0$	$2\Gamma_1$
$A_g(1)$	128.72 ± 0.07	0.49 ± 0.02	2.06 ± 0.06	0.23 ± 0.02
$A_g(4)$	201.51 ± 0.06	1.21 ± 0.02	4.67 ± 0.07	0.53 ± 0.03
$B_{3g}(2)$	143.82 ± 0.07	0.87 ± 0.02	6.4 ± 0.1	0.41 ± 0.04

IV. CONCLUSIONS

We present a polarization-resolved Raman scattering study of NaFe$_{0.53}$Cu$_{0.47}$As single crystals. We observe four A_g and four B_{3g} phonon modes, at 126, 172, 183, and 197 cm^{-1} and 101, 139, 173, 226 and cm^{-1}, respectively. The results are consistent with the *Ibam* space-group symmetry structure, where Fe/Cu atoms form a stripe order.

No phonon anomaly is observed across the magnetic phase transition from 250 to 60 K, suggesting weak electron-phonon and magnetoelastic interaction.

[1] G. F. Chen, W. Z. Hu, J. L. Luo, and N. L. Wang, Phys. Rev. Lett. **102**, 227004 (2009).

[2] J. D. Wright, T. Lancaster, I. Franke, A. J. Steele, J. S. Möller, M. J. Pitcher, A. J. Corkett, D. R. Parker, D. G. Free, F. L. Pratt, P. J. Baker, S. J. Clarke, and S. J. Blundell, Phys. Rev. B **85**, 054503 (2012).

[3] A. F. Wang, J. J. Lin, P. Cheng, G. J. Ye, F. Chen, J. Q. Ma, X. F. Lu, B. Lei, X. G. Luo, and X. H. Chen, Phys. Rev. B **88**, 094516 (2013).

[4] G. Tan, Y. Song, R. Zhang, L. Lin, Z. Xu, L. Tian, S. Chi, M. K. Graves-Brook, S. Li, and P. Dai, Phys. Rev. B **95**, 054501 (2017).

[5] C. Ye, W. Ruan, P. Cai, X. Li, A. Wang, X. Chen, and Y. Wang, Phys. Rev. X **5**, 021013 (2015).

[6] Y. Song, Z. Yamani, C. Cao, Y. Li, C. Zhang, J. S. Chen, Q. Huang, H. Wu, J. Tao, Y. Zhu, W. Tian, S. Chi, H. Cao, Y.-B. Huang, M. Dantz, T. Schmitt, R. Yu, A. H. Nevidomskyy, E. Morosan, Q. Si, and P. Dai, Nat. Commun. **7**, 13879 (2016).

[7] C. E. Matt, N. Xu, B. Lv, J. Ma, F. Bisti, J. Park, T. Shang, C. Cao, Y. Song, A. H. Nevidomskyy, P. Dai, L. Patthey, N. C. Plumb, M. Radovic, J. Mesot, and M. Shi, Phys. Rev. Lett. **117**, 097001 (2016).

[8] A. Charnukha, Z. P. Yin, Y. Song, C. D. Cao, P. Dai, K. Haule, G. Kotliar, and D. N. Basov, Phys. Rev. B **96**, 195121 (2017).

[9] M. A. Tanatar, N. Spyrison, K. Cho, E. C. Blomberg, G. Tan, P. Dai, C. Zhang, and R. Prozorov, Phys. Rev. B **85**, 014510 (2012).

[10] X. Wang, Q. Liu, Y. Lv, Z. Deng, K. Zhao, R. Yu, J. Zhu, and C. Jin, Sci. China: Phys. Mech. Astron. **53**, 1199 (2010).

[11] E. Kroumova, M. Aroyo, J. Perez-Mato, A. Kirov, C. Capillas, S. Ivantchev, and H. Wondratschek, Phase Transit. **76**, 155 (2003).

[12] A. Gozar, Ph.D. thesis, University of Illinois at Urbana-Champaign, 2004.

[13] In the setup (see Fig. 2.1 in [12]) a Melles Griot Glan-Taylor polarizing prism with a better than 10^{-5} extinction ratio was used to clean the laser excitation beam and a Karl Lambrecht Corporation broad-band polarizing cube with an extinction ratio better than 1:500 was used for the analyzer.

[14] W.-L. Zhang, Z. P. Yin, A. Ignatov, Z. Bukowski, J. Karpinski, A. S. Sefat, H. Ding, P. Richard, and G. Blumberg, Phys. Rev. B **93**, 205106 (2016).

[15] S.-F. Wu, W.-L. Zhang, L. Li, H.-B. Cao, H.-H. Kung, A. S. Sefat, H. Ding, P. Richard, and G. Blumberg, arXiv:1712.01903.

[16] M. Klein, in *Light Scattering in Solids II. Basic Concepts and Instrumentation*, edited by M. Cardona and G. Gfintherodt (Springer, Berlin, 1982), Chap. 2.

[17] Y. J. Um, J. T. Park, B. H. Min, Y. J. Song, Y. S. Kwon, B. Keimer, and M. Le Tacon, Phys. Rev. B **85**, 012501 (2012).

[18] J. Menéndez and M. Cardona, Phys. Rev. B **29**, 2051 (1984).